Metal–Boron Nanotubes

DOI: 10.1002/ange.200602610

Noncrystalline Metal–Boron Nanotubes: Synthesis, Characterization, and Catalytic-Hydrogenation Properties**

Yan Zhu, Fuping Liu, Weiping Ding, Xuefeng Guo,* and Yi Chen*

Much attention has been focused recently on one-dimensional (1D) nanostructures, such as nanowires, nanorods, nanobelts, and nanotubes owing to their unique applications in, for example, energy storage, transistors, biochips, sensors. Several different synthetic strategies have been explored for generating 1D nanostructures, for example, self-assembly of 0D building blocks and size reduction of 1D microstructures.[1,2] Furthermore, appropriate capping reagents have been used to control the growth rates of various facets of a solid kinetically.[3] In the vapor–-liquid–-solid (VLS) process, the symmetry is broken by the introduction of a flat solid–liquid interface.[4] The supersaturation of a system can also be controlled below a certain level to effectively induce 1D growth.[5] Since the discovery of carbon nanotubes,[6] a variety of inorganic nanotubes have also been synthesized,[7–16] and template-directed methods have been found to be an elegant and straightforward route for the formation of nanotubular materials.[17–21]

Noncrystalline transition-metal–boron alloys with short-range-ordered and long-range-disordered structures have been intensively investigated owing to their important practical or potential applications in various fields, such as ferrofluids, powder metallurgy, magnetic applications, composite materials, and catalysis.[22–24] Although noncrystalline metal–boron alloys prepared by melt-quenching or chemical reduction date back to the 1950s—pure boron nanotubes have been reported only recently[9–11]—no studies have been reported on the chemical preparation of 1D morphologies of noncrystalline metal–boron alloys. Considering the unusual characteristics of these artificially synthesized 1D nanostructures, it is desirable to explore methods to obtain 1D noncrystalline metal–boron (M–B) alloys. Owing the isotropic structures of noncrystalline alloys it is difficult for them to be grown into 1D nanostructures. Herein we report the first synthesis of nanotubes of noncrystalline M–B (M = Fe, Co, and Ni) alloys involving the use of lyotropic liquid crystals (LCs) of non-ionic–anionic mixed surfactants as templates. The non-ionic surfactants used are Tween 40 (polyoxyethylene sorbitan monopalmitate), Tween 60 (polyoxyethylene sorbitan monostearate), and Tween 80 (polyoxyethylene sorbitan monooleate), and the anionic surfactant is CSA (camphorsulfonic acid). The noncrystalline M–B nanotubes thus prepared are more effective than the corresponding nanoparticles for the catalytic hydrogenation of *m*-nitrotoluene.

Figure 1a shows the X-ray diffraction (XRD) patterns of the as-synthesized nanotubes of noncrystalline M–B alloys. The three samples keep their noncrystalline features, as indicated by a broad peak located at a 2θ value of around 45° and the lack of other diffraction peaks from crystalline phases.[25]

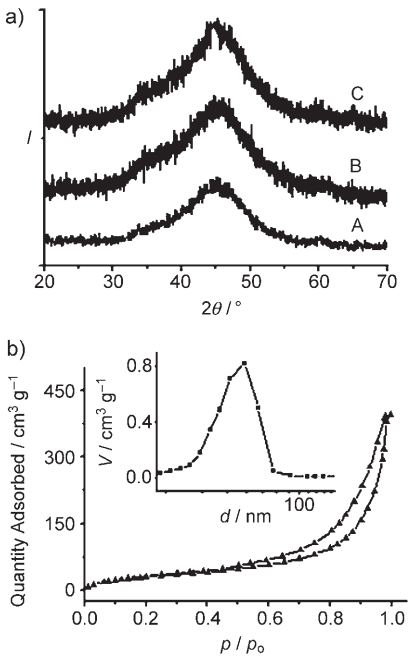

Figure 1. a) XRD patterns of Fe–B (A), Co–B (B), and Ni–B (C) nanotubes; b) nitrogen absorption isotherms of Fe–B nanotubes measured at 77 K; the inset shows the corresponding pore size distribution curve determined by the BJH method from the desorption isotherm; V = pore volume, d = pore width.

Figure 1b shows the N_2 sorption isotherms and pore size distribution of Fe–B nanotubes; similar results were obtained for Co–B and Ni–B nanotubes. The porous characteristics of the three noncrystalline M–B alloys are summarized in Table 1. Their surface areas measured by N_2 sorption are basically consistent with those evaluated from the size of the nanotubes measured by transmission electron microscopy (TEM).

These noncrystalline nanotubes are fragile under high-energy electron-beam irradiation. Therefore a low voltage of 80 kV was adopted for most of the TEM measurements. Unfortunately, such a low voltage can only provide the

[*] Y. Zhu, Prof. W. Ding, Prof. X. Guo, Prof. Y. Chen
Lab of Mesoscopic Chemistry
School of Chemistry and Chemical Engineering
Nanjing University
Nanjing 210093 (P.R. China)
Fax: (+86) 258-331-7761
E-mail: dingwp@nju.edu.cn
guoxf@nju.edu.cn
Dr. F. Liu
Changzhou Sunlight Fine Chemical Co., Ltd.
Changzhou 213134 (P.R. China)

[**] We are grateful for financial support from MOST (China) (grant no. 2003CB615804) and the NSF (China) (grant no. 20403008).

Table 1: Porous texture of the samples detected by N_2 sorption isotherms,[a] and their catalytic performance for the hydrogenation of *m*-nitrotoluene to *m*-toluidine.[b]

Samples	S_{BET} [$m^2 g^{-1}$]	Pore size [nm]	Pore volume [$cm^3 g^{-1}$]	Yield [%]
Fe–B NTs	118.3	46.2	0.6	79.2
Co–B NTs	98.9	55.9	0.5	93.8
Ni–B NTs	92.6	59.7	0.5	93.1
Fe–B NPs	39.6	10.2	0.2	10.7
Co–B NPs	33.5	10.6	0.1	83.5
Ni–B NPs	31.9	8.2	0.1	80.0
Pd/C (3%)	1100.1	–	–	96.0

[a] Surface area: BET method; pore diameter: BJH method from the desorption branch; pore volume: single-point adsorption total pore volume at a relative pressure of 0.97. NTs: nanotubes; NPs: nanoparticles prepared according to ref. [26]. [b] The reaction was performed at 393 K and 2.0 MPa of hydrogen pressure for 2 h for all samples except Fe–B NTs and NPs, for which a hydrogen pressure of 3.5 MPa was used.

morphology of the nanotubes (as shown in Figure 2a) rather than any further details regarding their local structures. TEM images (Figure 2a) of Fe–B nanotubes prepared using Tween 40 and CSA as template reveal that the nanotubes are several micrometers in length and have inner and outer diameters of around 50–55 and 60–65 nm, respectively. The continuous broad halo rings (inset of Figure 2a) resulting from selected-area electron diffraction (SAED) further support the noncrystalline nature of the Fe–B nanotubes and are consistent with the magnified TEM image taken at 200 kV shown in Figure 2b. To avoid damaging the nanotubes this image was taken in the shortest possible time. Energy dispersive spectrometry (EDS) of a single nanotube revealed the coexistence of Fe and B in the sample at an atomic ratio

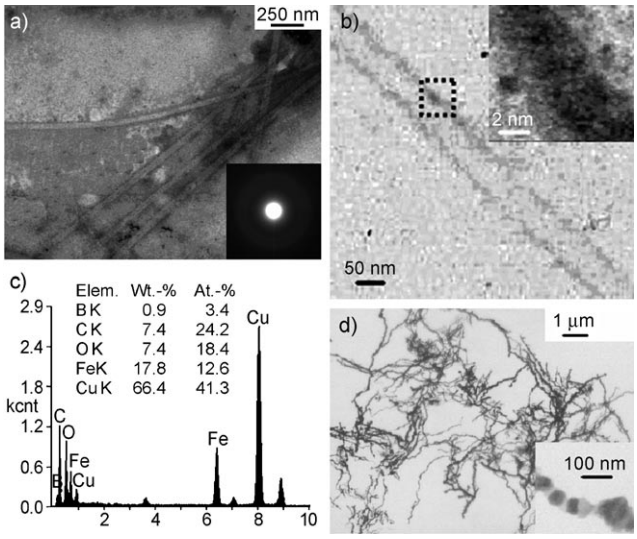

Figure 2. a) TEM image (80 kV) of Fe–B nanotubes; inset: the corresponding SAED pattern; b) HRTEM image (200 kV) of one isolated Fe–B nanotube inset: expansion of marked section; c) EDS spectrum of a single Fe–B nanotube (kcnt = kilocounts); d) TEM image of Fe–B noncrystalline chains of beads obtained with only CSA as the template, inset: enlargement.

about 3.7:1 (Figure 2c). In contrast, when only CSA was used as surfactant chains were observed resulting from assembly of nanoparticles through the magnetism of Fe–B (Figure 2d), whereas with Tween 40, Tween 60, or Tween 80 as the sole template sheet-like structures were obtained (not shown).

The Co–B and Ni–B nanotubes obtained with Tween 60 and CSA as template are also noncrystalline. Their TEM, SAED, and EDS images (Figure 3) reveal the noncrystalline

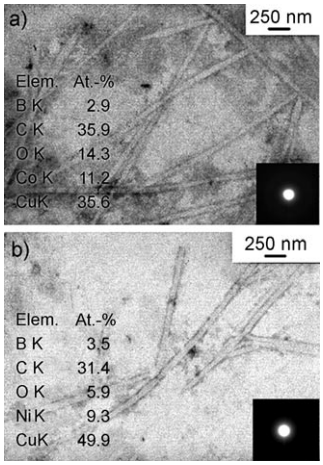

Figure 3. TEM images (80 kV) and corresponding SAED (inset) and EDS analyses of a) Co–B nanotubes and b) Ni–B nanotubes.

nature of these nanotubes and the reasonable M:B ratios obtained. Elemental analysis by inductively coupled plasma (ICP) spectroscopy indicated that the Fe:B, Co:B, and Ni:B atomic ratios in the as-prepared samples are 3.2:1, 2.9:1, and 2.5:1, respectively, which are basically consistent with the EDS results and are close to the composition of the nanoparticulate counterparts selected for comparison.[26]

A few M–B nanoparticles can often be seen in the TEM images of the noncrystalline nanotube samples. It seems difficult to avoid having these nanoparticles present, this is tentatively attributed to there being only weak interactions between the metal ions and surfactants in the soft-template method used. However, the noncrystalline nanotubes are always the major product, with an estimated percentage of more than 70% according to microscopic observation on various samples.

The template has a strong impact on the morphology of the product. It is likely that the lyotropic nematic nature of the non-ionic–anionic surfactant mixture provides a template for the growth of 2D lamellar mesostructures, and the synthesis of the nanotubes might consist of two steps. The first step should be the formation of a lamellar structure by the condensation of the mixed surfactants and metal cations. The cations are likely to be located in the spaces between the head groups of the anionic surfactant. This arrangement is a result of the formation of CSA–M ion pairs stabilized by the non-ionic surfactant LCs, and means that the metallic ions are confined to the aqueous interface of the mixed-surfactant lamellar micelles. The second step, which is induced by the addition of sodium borohydride, is the reduction of these metal ions, which results in the loosening of the lamellar

nanosheets and the rolling-up of the 2D nanosheets, driven by a decrease in their surface free energy, similar to the formation of cylindrical nanotubes from layered materials. The reduction process is strongly exothermic and is responsible for the ultimate formation of nanotubular M–B alloys. However, one question remains unanswered, namely why different Tween surfactants have to be used for different M–B nanotubes (Tween 40 gives Fe–B and Tween 60 gives Co–B and Ni–B, while Tween 80 is not effective at all). This observation suggests that the interactions between the transition-metal ions and surfactants are rather complicated and probably vary with the nature of the metal ion.

Noncrystalline metal–boron alloys have been used as hydrogenation catalysts for a long time and their use in magnetically stabilized bed reactors for hydrogenation reactions has made great progress recently.[27] To elucidate the shape-specific effects of nanotubes, the ability of our noncrystalline nanotubes to catalyze the hydrogenation of *m*-nitrotoluene was investigated (see Table 1; the catalytic properties of noncrystalline M–B nanoparticles are also included for comparison). When Fe–B nanotubes were employed as the catalyst the yield of *m*-toluidine in the first reaction cycle was 79.2%, compared with 10.7% for conventional Fe–B nanoparticles under the same reaction conditions. The catalytic activity of the noncrystalline Fe–B nanotubes is evidently much higher than that of Fe–B nanoparticles. The higher catalytic activity of the nanotubes can be partially ascribed to their larger surface area, although this cannot entirely account for the better catalytic performance of the nanotubes. The structure of the nanotube must also have some effect. The negative curvature of the nanotube's inner surface may enhance the coordination of reaction molecules by the multiple active centers. Gubbins et al. have simulated the chemical reaction of N_2 and three equivalents of H_2 under confining conditions, especially in nanotubes, and have found that the fluid molecules in the nanotubes experience a strong interaction with the walls.[28,29] In the current hydrogenation reaction the noncrystalline alloy catalysts strongly adsorb hydrogen, and *m*-nitrotoluene, which is capable of wetting and selectively adsorbing onto the solid surfaces, should experience a large attractive potential energy because of the combined interactions in the tubes. These effects must affect the reaction equilibrium and result in an increase in the yield of *m*-toluidine through Le Chatelier's principle as a result of the decrease in the total number of molecules in the reaction system.[30]

Noncrystalline Co–B and Ni–B nanotubes provide an interesting comparison with the Fe–B nanotubes since the primary factors determining their activity are somewhat different. Conventional noncrystalline Co–B and Ni–B nanoparticles display high resistivity to poisoning as well as good activity and selectivity for certain hydrogenation reactions. Consequently, the increased surface area and nanotube effects cause an increase of *m*-toluidine yields for these two nanotube samples, although this increase is not as remarkable as for the Fe–B nanotubes. As seen from Table 1, the catalytic activities of Co–B and Ni–B nanotubes are similar to that of Pd/C (Pd content of 3% and a surface area of 1100 $m^2 g^{-1}$.). Figure 4 shows the TEM image and the corresponding SAED and EDS results for the Fe–B nanotubes after two catalytic cycles. (The yield of *m*-toluidine in the second cycle is 75.3%.) The structure of the nanotubes appears to have changed very little after two catalytic cycles. The nanotubular morphologies are still observed and their structures are still noncrystalline, as determined by SAED. These results are inspiring and further work in this area is in progress.

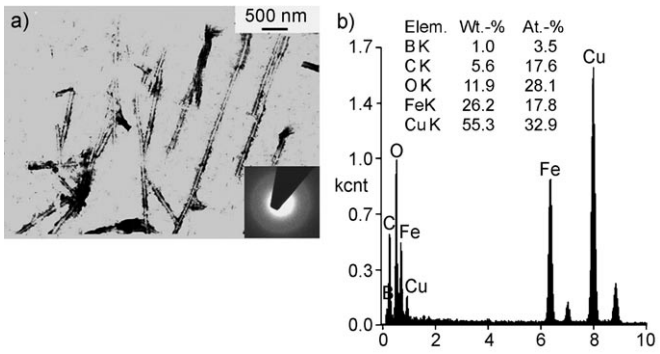

Figure 4. TEM image (a) and EDS spectrum (b) of Fe–B nanotubes after two catalytic cycles. The inset of (a) is the corresponding SAED pattern.

In summary, metal–boron nanotubes with a uniform size have been fabricated by using lyotropic non-ionic–anionic mixed-surfactant liquid crystals as templates. This method provides a route for the synthesis of metal–boron nanotubes and can also be extended to other tubular materials or noncrystalline alloys. The results of catalytic studies show that these metal–boron nanotubes exhibit superior catalytic activities to the corresponding metal–boron nanoparticles. They are therefore promising for future applications in catalysis and might become a new class of industrial material.

Experimental Section

In a typical synthesis, $FeCl_3 \cdot 6H_2O$ (0.01 mol, 2.7 g) was dissolved in H_2O (18 mL) containing (1*S*)-(+)-10-camphorsulfonic acid (0.01 mol, 2.3 g) and Tween 40 (0.01 mol, 12.8 g) at 333 K. The mixture was then cooled to 293 K and allowed to stand at that temperature for 1 h. A mixture of 4 M $NaBH_4$ and 0.1 M NaOH was added to the above homogeneous mixture and kept for 48 h under an inert gas atmosphere (N_2). The resulting solid was collected, washed with distilled water and ethanol, and dried in flowing nitrogen. The noncrystalline Co–B and Ni–B nanotubes were prepared from $CoCl_2 \cdot 6H_2O$ or $NiCl_2 \cdot 6H_2O$ and Tween 60 in place of $FeCl_3 \cdot 6H_2O$ and Tween 40 under otherwise identical experimental conditions.

Hydrogenation of *m*-nitrotoluene was used to measure the catalytic performance. Thus, a 250-mL autoclave loaded with methanol (200 mL), *m*-nitrotoluene (10 g, 0.07 mol), and catalyst (0.5 g, 0.008 mol) was filled with hydrogen (2 MPa; 3.5 MPa was used for Fe–B) after purging to remove air, stirred vigorously, and heated to 393 K. After 2 h the products were analyzed by gas chromatography.

Powder XRD measurements were performed with a Philips X'Pert MPD Pro X-ray diffractometer with graphite-monochromated high-intensity $Cu_{K\alpha}$ radiation at 50 kV. TEM and EDS images were recorded with a JEM-100S Electron Microscope (JEOL) at an accelerating voltage of 80 kV. HRTEM was performed with a JEOL JEM-2010 instrument at an acceleration voltage of 200 kV. An aliquot of the sample suspended in ethanol was dropped on a polymer-coated copper grid for TEM observation. ICP spectroscopy was performed

with a J-A1100 spectrometer (Jarrell–Ash). The nitrogen sorption isotherms were measured at liquid-nitrogen temperature on an ASAP 2020 apparatus.

Received: June 30, 2006
Revised: August 7, 2006
Published online: October 9, 2006

Keywords: alloys · heterogeneous catalysis · liquid crystals · nanotubes · surfactants

[1] C. A. Mirkin, R. L. Letsinger, R. C. Mucic, J. J. Storhoff, *Nature* **1996**, *382*, 607.
[2] R. M. Penner, M. J. Heben, T. L. Longin, N. S. Lewis, *Science* **1990**, *250*, 1118.
[3] X. G. Peng, L. Manna, W. D. Yang, J. Wickham, E. Scher, A. Kadavanich, A. P. Alivisatos, *Nature* **2000**, *404*, 59.
[4] J. D. Holmes, K. P. Johnston, R. C. Doty, B. A. Korgel, *Science* **2000**, *287*, 1471.
[5] X. Wang, Y. Li, *J. Am. Chem. Soc.* **2002**, *124*, 2880.
[6] S. Iijima, *Nature* **1991**, *354*, 56.
[7] N. G. Chopra, R. J. Ruyken, K. Cherry, V. H. Crespi, M. L. Cohen, S. G. Louie, A. Zettl, *Science* **1995**, *269*, 966.
[8] R. Ma, Y. Bando, D. Golberg, T. Sato, *Angew. Chem.* **2003**, *115*, 1880; *Angew. Chem. Int. Ed.* **2003**, *42*, 1836.
[9] D. Ciuparu, R. F. Klie, Y. Zhu, L. Pfefferle, *J. Phys. Chem. B* **2004**, *108*, 3967.
[10] A. Quandt, A. Y. Liu, I. Boustani, *Phys. Rev. B* **2001**, *64*, 125422.
[11] A. Quandt, I. Boustani, *ChemPhysChem.* **2005**, *6*, 2001.
[12] W. Tremel, *Angew. Chem.* **1999**, *111*, 2311; *Angew. Chem. Int. Ed.* **1999**, *38*, 2175.
[13] G. R. Patzke, F. Krumeich, R. Nesper, *Angew. Chem.* **2002**, *114*, 2554; *Angew. Chem. Int. Ed.* **2002**, *41*, 2446.
[14] R. Tenne, *Angew. Chem.* **2003**, *115*, 5280; *Angew. Chem. Int. Ed.* **2003**, *42*, 5124.
[15] M. Remskar, *Adv. Mater.* **2004**, *16*, 1497.
[16] R. Tenne, C. N. R. Rao, *Philos. Trans. R. Soc. London Ser. A* **2004**, *362*, 2099.
[17] C. R. Martin, *Science* **1994**, *266*, 1961.
[18] M. E. Spahr, P. Bitterli, R. Nesper, M. Muller, F. Krumeich, H. U. Nissen, *Angew. Chem.* **1998**, *110*, 1339; *Angew. Chem. Int. Ed.* **1998**, *37*, 1263.
[19] H. P. Lin, C. Y. Mou, S. B. Liu, *Adv. Mater.* **2000**, *12*, 103.
[20] Y. D. Li, X. L. Li, R. R. He, J. Zhu, Z. X. Deng, *J. Am. Chem. Soc.* **2002**, *124*, 1411.
[21] T. Kijima, T. Yoshimura, M. Uota, T. Ikeda, D. Fujikawa, S. Mouri, S. Uoyama, *Angew. Chem.* **2004**, *116*, 230; *Angew. Chem. Int. Ed.* **2004**, *43*, 228.
[22] W. L. Johnson, *Prog. Mater. Sci.* **1986**, *30*, 81.
[23] A. Molnar, G. V. Smith, M. Bartoâk, *Adv. Catal.* **1989**, *36*, 329.
[24] Y. Chen, *Catal. Today* **1998**, *44*, 3.
[25] S. Mûrup, S. A. Sethi, S. Linderoth, C. B. Koch, M. D. Bentzon, *J. Mater. Sci.* **1992**, *27*, 3010.
[26] J. Y. Shen, Z. Hu, L. F. Zhang, Z. Y. Li, Y. Chen, *Appl. Phys. Lett.* **1991**, *59*, 3545.
[27] X. K. Meng, X. H. Mu, B. N. Zong, E. Z. Min, Z. H. Zhu, S. B. Fu, Y. B. Luo, *Catal. Today* **2003**, *79*, 21.
[28] C. H. Turner, J. K. Johnson, K. E. Gubbins, *J. Chem. Phys.* **2001**, *114*, 1851.
[29] O. Byl, P. Kondratyuk, J. T. Yates, *J. Phys. Chem. B* **2003**, *107*, 4277.
[30] M. S. Bartkowiak, G. Dudziak, R. Sikorski, R. Gras, R. Rodhakrishnan, K. E. Gubbins, *J. Chem. Phys.* **2001**, *114*, 950.

